Available online at www.sciencedirect.com
SCIENCE DIRECT®
Journal of Computational and Applied Mathematics 170 (2004) 1–25
JOURNAL OF COMPUTATIONAL AND APPLIED MATHEMATICS
www.elsevier.com/locate/cam

Thermally enhanced gravity driven flows

S.J.D. D'Alessio[a,*], J.P. Pascal[b], T.B. Moodie[c]

[a] *Department of Applied Mathematics, University of Waterloo, Waterloo, Ontario, N2L 3G1, Canada*
[b] *Department of Mathematics, Physics and Computer Science, Ryerson University, Toronto, Ontario, M5B 2K3, Canada*
[c] *Applied Mathematics Institute, Department of Mathematical and Statistical Sciences, University of Alberta, Edmonton, Alberta T6G 2G1, Canada*

Received 25 February 2003; received in revised form 1 December 2003

Abstract

Gravity currents play a major role in both natural and human-made settings. The driving buoyancy forces for these flows are due to density differences which may arise as a result of compositional differences (e.g. salinity), the presence of suspended material in the flow as in the case of turbidity currents, temperature differences, or a combination of these mechanisms. This article reports on a study of surface gravity currents moving horizontally over a slightly denser ambient fluid when these surface layers are subjected to an incoming heat flux which acts to enhance (or erode) the existing stratification. A general equation of state is adopted to connect the density of the upper layer to its changing temperature. A two-layer hydraulic theory is developed and conditions for its validity carefully specified. Both analytical and numerical analyses are carried out in order to examine the salient features of these flows.

Keywords: Shallow-water theory; Hyperbolic conservation laws; Variable density, Two-layer model

1. Introduction

A gravity current consists of the flow of one fluid within another when this flow takes place because of differences in density between two fluids. In natural or human-made aquatic settings such as lakes, oceans or reservoirs there are a myriad of possible contributors to these density differences including: temperature differences, salinity contrasts, suspended material, both organic and inorganic (turbidity currents), as well as combinations of these mechanisms. In the arena of human activity,

* Corresponding author. Fax: +1-519-746-0274.
E-mail addresses: sdalessio@math.uwaterloo.ca (S.J.D. D'Alessio), jpascal@ryerson.ca (J.P. Pascal), bryant.moodie@ualberta.ca (T.B. Moodie).

0377-0427/$ - see front matter
doi:10.1016/j.cam.2003.12.037

gravity currents produced in the atmosphere or oceans may acquire their driving buoyancy force as a result of the accidental (or otherwise) release and subsequent suspension of industrial pollutants. This buoyancy force drives the spread of oil slicks on the sea surface [13] and are also pivotal in the formation of the so-called thermal bar in dimictic lakes [9]. In this latter example temperature differences produce the buoyancy force. Temperature differences arising from the absorption of solar radiation may also play a pivotal role in the spread of oil slicks. Buoyancy-driven flows are also being studied extensively with the aim of including their effects in design criteria for natural ventilation of buildings [19]. This relatively new systematic application of these compositionally-driven flows holds great promise for energy savings in future designs. Gravity flows are thus seen to be highly complex flows that are ubiquitous in nature and human activities and studies of them will be as varied in their aim as the manifestations of these currents themselves.

Gravity currents are primarily horizontal, occurring as either top or bottom boundary currents or as intrusions at some intermediate level. The majority of the theoretical work on gravity currents from the early calculation by von Kármán [26] up to that by Benjamin [2] and right on through into the mid 1980s dealt with compositionally-driven flows treating them as steady and employing a hydrostatic approximation. This hydraulic approach for fixed interlayer density differences will, however, not necessarily be valid for applications involving conditions such as rapid bed slope changes, strong stratification or short period waves. Under these circumstances extensions to shallow water theory may be required in order to gain sufficient accuracy [1]. In the cases where the density in either layer is variable extreme care must be taken in order to ensure that the use of shallow water theory is justified. For example, in the case of turbidity currents with sedimenting particles, horizontal gradients in particle concentration will rule out the use of hydraulic theory even for low aspect ratio flows [21].

Since our top boundary current will be subjected to some of the same dynamic balances as bottom boundary currents with relation to the reverse flow in the dense ambient fluid, we include a brief summary of findings from a set of experiments on time dependent compositionally-driven flows executed by Rottman and Simpson [24]. In these experiments they studied instantaneous releases for $0 < h_i \leqslant 1$, where h_i is the initial depth ratio between the released heavy fluid and the total depth of the two fluid system in the rectangular channel. In their work they focused on the flow's transition to the self-similar phase. The key feature of their observations and one that has played a role in all subsequent theoretical developments for bottom boundary currents, was that for h_i equal to or slightly less than unity the disturbance generated at the proximal end wall has the appearance of an internal hydraulic drop. On the other hand, for smaller values of h_i ($\lesssim 0.7$) this disturbance is a long wave of depression. Currently there are no theoretical model-based calculations that can accurately predict this bifurcation in behaviour which occurs in the experimental results as h_i is varied. These experiments did however serve to emphasize the importance of including the effects of the ambient fluid on the bottom boundary current when the current initially occupies a large fraction of the total depth.

D'Alessio et al. [5] employed a two layer shallow water model to study sudden releases for fixed volumes entering a lighter ambient fluid as a bottom gravity flow. Using MacCormack's method [18] to integrate numerically the hyperbolic system they were able to achieve good qualitative agreement with the experimental results of Rottman and Simpson [24] for transition to self-similarity. Also, employing multiple scales arguments they were able to show analytically the dependence of internal bore formation on initial fractional depth of the release volume. Their analysis, however, did not

confirm the value of $h_i \simeq 0.7$ referred to earlier but rather gave the lower value of $h_i = 0.5$ as the minimum fraction for bore initiation. This is perhaps not surprising when one contrasts the relative simplicity of a shallow water (hydraulic) model for what is a complex flow involving possible nonhydrostatic effects in various regions of the flow due to streamline curvature, unresolved small scale dissipation and other effects.

In this article we develop a two layer model governing the sudden release of a fixed volume of light fluid whose initial density and temperature are ρ_1 and T_1, respectively, into a heavy ambient fluid of density $\rho_2 > \rho_1$ overlying a mildly sloping bottom. We shall assume that the temperature and hence density of this ambient fluid remains fixed. This is consistent with the assumption that there is no heat transferred into the bottom layer. The lighter upper fluid layer is assumed to be subjected to an incoming heat flux (such as radiation) which serves to enhance (or erode) the initial stratification through volume changes. In the case of heating the enhanced stratification inhibits turbulent mixing [23]. The neglect of viscous dissipation in the flow stems from the assumption that the Reynolds number is sufficiently large [23].

2. Formulation

Consider a current produced by the release of a fixed volume of fluid having initial density $\rho_1 = \rho_*$ into an ambient fluid of higher density $\rho_2 = \rho_0$ overlying a gently sloping bottom. The physical configuration is depicted in Fig. 1, where $\eta(x,t)$ represents the displacement of the free surface from its undisturbed configuration, (u,w) is the fluid velocity in Cartesian coordinates (x,z), H is the mean depth of the two layer system measured from $z = 0$, $h(x,t)$ is the thickness of the overlying layer and the variable bottom is located at $z = -sf(x)$, where s $(0 < s \ll 1)$ is a nondimensional

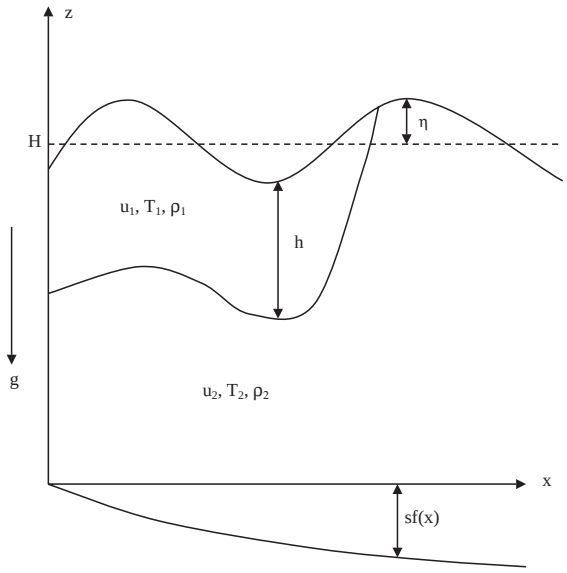

Fig. 1. The flow configuration of the two-layer fluid model.

slope parameter. The flow is driven by the buoyancy force arising because of the difference between the temperature dependent density $\rho_1(T)$ of the upper layer and the fixed density $\rho_2 = \rho_0$ of the ambient fluid. The relation between temperature and density for the upper layer is given in terms of an equation of state which will be assumed to have the general form [20]

$$\rho_1(T) = \rho_0[1 - \alpha(T - T_0)^n], \tag{2.1}$$

wherein T_0 is the fixed temperature of the lower layer whose density is also fixed at ρ_0, α is the thermal expansion coefficient, and $n > 0$ is a power law index. Since the temperature of the lower layer is assumed to remain fixed we have chosen to measure the temperature $T_1 \equiv T$ of the upper layer relative to this fixed value. We shall take $T_* > T_0$ as the initial temperature of the upper layer so that

$$\rho_1(T_*) = \rho_* = \rho_0[1 - \alpha(T_* - T_0)^n] < \rho_0. \tag{2.2}$$

While in much of this study n will be treated as a free parameter, detailed numerical results will be presented for the special cases $n=1$ and 2 since these are natural choices. The case $n=1$ corresponds to the usual description whereby the density decreases linearly with an increase in temperature [15]. The case $n = 2$ can be used to approximate the density of fresh water near the temperature of maximum density, that is, $T_0 \approx 4°\mathrm{C}$ with $\alpha = 1.65 \times 10^{-5}°\mathrm{C}^{-2}$ for water. The case having $n = 0$ removes the temperature dependence from the problem so that the equations of motion would then be reduced in number by one and the problem would mirror the one analysed previously by Rottman and Simpson [24] as well as by D'Alessio et al. [5] for bottom flows.

Invoking the Boussinesq approximation gives for mass conservation in the upper (variable density) and lower (fixed density) layers

$$\frac{\partial u_1}{\partial x} + \frac{\partial w_1}{\partial z} = 0, \tag{2.3}$$

$$\frac{\partial u_2}{\partial x} + \frac{\partial w_2}{\partial z} = 0, \tag{2.4}$$

respectively. In all that follows we further assume that the Reynolds number of the flow is sufficiently large that viscous forces are negligible and that the flow dynamics are dominated by a balance between buoyancy and inertial forces. The equation of momentum balance in each layer then takes the relatively simple vector form

$$\rho \frac{D\mathbf{u}}{Dt} = -\nabla p + \rho \mathbf{g}, \tag{2.5}$$

wherein p is the total fluid pressure and $\mathbf{g}$ the gravitational acceleration vector with ρ for the upper layer taking the variable value $\rho_1(T)$ specified by (2.1).

We now adapt Eqs. (2.3)–(2.5) to study low aspect ratio flows involving two coupled layers consisting of an upper layer having a temperature dependent (and hence time dependent) density overlying a homogenous fluid layer of fixed density that is in contact with a gently sloping impermeable bottom.

The momentum equations for the upper layer may be written as

$$\frac{\partial u_1}{\partial t} + u_1 \frac{\partial u_1}{\partial x} + w_1 \frac{\partial u_1}{\partial z} = -\frac{1}{\rho_0} \frac{\partial p_1^*}{\partial x}, \tag{2.6}$$

$$\frac{\partial w_1}{\partial t} + u_1 \frac{\partial w_1}{\partial x} + w_1 \frac{\partial w_1}{\partial z} = -\frac{1}{\rho_0} \frac{\partial p_1^*}{\partial z}, \tag{2.7}$$

where the total pressure in the upper layer has been expressed as

$$p_1(x,z,t) = -\rho_0[1 - \alpha(T - T_0)^n]gz + p_1^*(x,z,t), \tag{2.8}$$

with p_1^* representing the dynamic pressure field in the upper layer and a Boussinesq approximation has been invoked. This decomposition allows us to eliminate the time dependent gravitational force per unit mass from the vertical momentum equation (2.7). It should be emphasized, however, that if the density in the upper layer varied in the horizontal coordinate then this decomposition would not have been possible and the upper layer would no longer be in hydrostatic balance [23]. Developing a hydraulic model therefore imposes fairly strong constraints on the heating/cooling of the upper layer.

The idea behind this hydraulic approximation when applied to a layer of fluid is that to $O(\delta^2)$ in the small parameter δ the pressure is hydrostatic. This small parameter is known as the aspect ratio [22] defined as

$$0 < \delta \equiv \frac{h_0}{L} \ll 1, \tag{2.9}$$

with h_0 a vertical scale of the motion and L a horizontal scale. Standard scaling arguments applied to the vertical momentum equation for the upper fluid layer give that

$$\frac{\partial p_1}{\partial z} = -\rho_0[1 - \alpha(T - T_0)^n]g + O(\delta^2), \tag{2.10}$$

and hence $\partial p_1^*/\partial z = 0$ to $O(\delta^2)$. Integrating (2.10) and applying the boundary condition of vanishing pressure at the free surface $z = H + \eta$ gives

$$p_1 = \rho_0 g[1 - \alpha(T - T_0)^n](H + \eta - z). \tag{2.11}$$

From (2.11) we have that the horizontal velocity in the upper layer will be independent of z. If, however, the temperature and hence the density of this layer should vary in the horizontal coordinate then the velocity field will be depth dependent and shallow water theory violated.

Since our assumption of a spatially independent temperature field provides for a depth independent horizontal velocity field in the upper layer, the horizontal momentum equation for that layer becomes

$$\frac{\partial u_1}{\partial t} + u_1 \frac{\partial u_1}{\partial x} + g[1 - \alpha(T - T_0)^n] \frac{\partial \eta}{\partial x} = 0. \tag{2.12}$$

Integrating the continuity equation (2.3) and applying the kinematic boundary conditions at the lower and upper boundaries of the upper layer gives the continuity equation for that layer as

$$\frac{\partial h}{\partial t} + \frac{\partial}{\partial x}(hu_1) = 0. \tag{2.13}$$

The momentum equations for the lower layer are now

$$\frac{\partial u_2}{\partial t} + u_2 \frac{\partial u_2}{\partial x} + w_2 \frac{\partial u_2}{\partial z} = -\frac{1}{\rho_0} \frac{\partial p_2^*}{\partial x}, \tag{2.14}$$

$$\frac{\partial w_2}{\partial t} + u_2 \frac{\partial w_2}{\partial x} + w_2 \frac{\partial w_2}{\partial z} = -\frac{1}{\rho_0} \frac{\partial p_2^*}{\partial z}, \tag{2.15}$$

where the total pressure field in the lower layer has been expressed as

$$p_2(x,z,t) = -\rho_0 g z + p_2^*(x,z,t), \tag{2.16}$$

with p_2^* being the dynamic pressure field in the lower layer.

From (2.11) and (2.16) and the dynamic condition that the total pressure field across the interface at $z = H + \eta - h$ must be continuous we have that

$$p_2 = \rho_0 g[H + \eta - z - \alpha h (T - T_0)^n]. \tag{2.17}$$

From (2.17) we have, following the arguments employed for the upper layer, that $u_2 = u_2(x,t)$ and hence that the horizontal momentum equation for the lower layer is

$$\frac{\partial u_2}{\partial t} + u_2 \frac{\partial u_2}{\partial x} + g \frac{\partial \eta}{\partial x} - \alpha g (T - T_0)^n \frac{\partial h}{\partial x} = 0. \tag{2.18}$$

The continuity equation (2.4) may now be integrated and the kinematic boundary conditions applied to give

$$\frac{\partial}{\partial t}(h - \eta) + \frac{\partial}{\partial x}[(h - H - \eta - s f(x)) u_2] = 0. \tag{2.19}$$

Our equations of motion now consist of (2.12), (2.13), (2.18) and (2.19) together with a heat equation yet to be specified. We shall now render in nondimensional form the above four equations by introducing the nondimensional variables (denoted by a tilde) as follows:

$$x = L\tilde{x}, \quad z = h_0 \tilde{z}, \quad t = \frac{L}{U}\tilde{t}, \quad h = h_0 \tilde{h}, \quad H = h_0 \tilde{H},$$

$$(u_1, u_2) = U(\tilde{u_1}, \tilde{u_2}), \quad (w_1, w_2) = \frac{h_0 U}{L}(\tilde{w_1}, \tilde{w_2}), \quad (p_1^*, p_2^*) = U^2 \rho_0 (\tilde{p_1^*}, \tilde{p_2^*}),$$

$$\eta = \frac{U^2}{g}\tilde{\eta}, \quad s = \delta \tilde{s}, \quad \theta = T - T_0 = \theta_0 \tilde{\theta}, \quad U^2 = g' h_0. \tag{2.20}$$

In (2.20), θ_0 is a temperature scale which we choose to be the initial temperature difference between the two layers so that $\theta_0 = T_* - T_0 > 0$. Employing this scheme to nondimensionalize our four equations of motion we obtain

$$\frac{\partial u_1}{\partial t} + u_1 \frac{\partial u_1}{\partial x} + \left[1 - \frac{g'}{g}\theta^n\right] \frac{\partial \eta}{\partial x} = 0, \tag{2.21}$$

$$\frac{\partial h}{\partial t} + \frac{\partial}{\partial x}(h u_1) = 0, \tag{2.22}$$

$$\frac{\partial u_2}{\partial t} + u_2 \frac{\partial u_2}{\partial x} + \frac{\partial \eta}{\partial x} - \theta^n \frac{\partial h}{\partial x} = 0, \tag{2.23}$$

$$\frac{\partial}{\partial t}\left(h - \frac{g'}{g}\eta\right) + \frac{\partial}{\partial x}\left[\left(h - H - \frac{g'}{g}\eta - sf(x)\right)u_2\right] = 0, \tag{2.24}$$

where tildes have been dropped from nondimensional quantities for notational convenience. The reduced gravity g' introduced above is defined in terms of the initial density difference between the two layers, that is

$$g' = \frac{\rho_0 - \rho_*}{\rho_0} g = \alpha\theta_0^n g. \tag{2.25}$$

It now remains for us to specify a heat equation for the temperature field in the upper layer. This heat equation may be written in terms of θ as

$$\frac{\partial \theta}{\partial t} + u_1 \frac{\partial \theta}{\partial x} + w_1 \frac{\partial \theta}{\partial z} = \kappa \nabla^2 \theta + Q, \tag{2.26}$$

where u_1, w_1 are as previously defined, κ is the thermal diffusivity, and Q the heat source term which we assume to be independent of x. This assumption is consistent with a spatially uniform heat flux on the surface of the upper layer and as was mentioned earlier leads to a very significant simplification of the model equations in that a hydraulic model applies. With Q independent of x the temperature field and hence the density of the upper layer will also be independent of x. Adopting the well-mixed assumption of Zilitinkevich et al. [28] for the upper layer leads to a depth independent temperature field so that $\partial\theta/\partial z = 0$ and $\nabla^2\theta = 0$ so that our nondimensional heat equation reduces to

$$\frac{\mathrm{d}\theta}{\mathrm{d}t} = Q(t), \quad \left(Q = \frac{U\theta_0}{L}\tilde{Q}\right). \tag{2.27}$$

Lastly, we point out that implicit in the assumption that there is no heat transfer between the two layers is the criterion that the diffusive, or convective, time scale given by $t_d \sim h_0^2/\kappa$ is much larger than the advective time scale L/U. This condition places constraints on the quantities h_0 and L for a given fluid having a specified κ.

Our dynamic equations now consist of (2.21)–(2.24) and (2.27). This set of equations contains the parameters g'/g, s and H. The parameter g'/g is a measure of the importance of the free surface on the flow since letting $g'/g \to 0$ filters out surface wave phenomena [5]. The slope parameter s determines the role of bottom topography in the flow. The parameter H is useful in considering the limiting case of a deep ambient layer as we shall shortly see. The system of equations (2.21)–(2.24) and (2.27) is posed as an initial value problem subject to the initial conditions

$$u_1(x,0) = 0, \quad u_2(x,0) = 0, \quad \eta(x,0) = 0, \quad h(x,0) = G(x), \quad \theta(0) = 1, \tag{2.28}$$

the impermeability conditions

$$u_1(0,t) = 0, \quad u_2(0,t) = 0, \tag{2.29}$$

the slope conditions

$$\frac{\partial \eta}{\partial x}(0,t) = \frac{\partial h}{\partial x}(0,t) = 0, \tag{2.30}$$

and the far-field conditions

$$u_1(x,t) \to 0, \quad u_2(x,t) \to 0, \quad \eta(x,t) \to 0, \quad h(x,t) \to 0, \tag{2.31}$$

as $x \to \infty$. The slope conditions (2.30) can easily be deduced from (2.21) and (2.23) by making use of the impermeability conditions. In the above $G(x)$ specifies the initial configuration of the two-layer fluid system which is taken to be initially at rest. We are interested in initial rectangular configurations of the form

$$G(x) = \begin{cases} h_* & \text{if } 0 \leqslant x \leqslant x_0, \\ 0 & \text{if } x > x_0, \end{cases} \tag{2.32}$$

where h_* is the nondimensional initial thickness of the surface gravity current. Lastly, the heat flux $Q(t)$ and the power law index n will need to be specified.

The first distinguished limit model to be developed is a *weakly stratified* model wherein we neglect terms of $O(g'/g)$ on the assumption that the initial density difference is small. This then gives the dynamic equations

$$\frac{\partial u_1}{\partial t} + u_1 \frac{\partial u_1}{\partial x} + \frac{\partial \eta}{\partial x} = 0, \tag{2.33}$$

$$\frac{\partial h}{\partial t} + \frac{\partial}{\partial x}(h u_1) = 0, \tag{2.34}$$

$$\frac{\partial u_2}{\partial t} + u_2 \frac{\partial u_2}{\partial x} + \frac{\partial \eta}{\partial x} - \theta^n \frac{\partial h}{\partial x} = 0, \tag{2.35}$$

$$\frac{\partial h}{\partial t} + \frac{\partial}{\partial x}[(h - H - s f(x)) u_2] = 0, \tag{2.36}$$

$$\frac{\mathrm{d}\theta}{\mathrm{d}t} = Q(t). \tag{2.37}$$

A series of straightforward manipulations of Eqs. (2.33)–(2.36) gives the pair of relations (with $s = 0$)

$$h u_1 + (H - h) u_2 = 0, \tag{2.38}$$

$$h u_1^2 + (H - h) u_2^2 + H\eta + \frac{\theta^n}{2}(H - h)^2 = 0, \tag{2.39}$$

from which we can obtain an expression for the deflection of the free surface as

$$\eta = \eta(u_1, h, \theta) = -\frac{u_1^2 h}{H - h} - \frac{\theta^n}{2H}(H - h)^2, \tag{2.40}$$

where we have used

$$u_2 = -\frac{h u_1}{H - h}. \tag{2.41}$$

Our weak stratification model can then be written in terms of the pair of equations

$$\frac{\partial u_1}{\partial t} + \left[1 - \frac{2h}{H-h}\right] u_1 \frac{\partial u_1}{\partial x} + \left[\frac{\theta^n}{H}(H-h) - \frac{u_1^2 H}{(H-h)^2}\right] \frac{\partial h}{\partial x} = 0, \tag{2.42}$$

$$\frac{\partial h}{\partial t} + \frac{\partial}{\partial x}(h u_1) = 0, \tag{2.43}$$

together with the heat equation (2.37) and the algebraic relation (2.41) for u_2.

Returning to our full set of model equations consisting of (2.21)–(2.24) together with the heat equation (2.27) we can develop another distinguished limit model for a *deep ambient layer* without making the weak stratification assumption. In (2.24) we let $H \to \infty$ with $h = \mathrm{O}(1)$ to get $u_2 = 0$ so that from (2.23)

$$\frac{\partial \eta}{\partial x} = \theta^n \frac{\partial h}{\partial x}. \tag{2.44}$$

Our system of equations for this deep ambient layer can then be written as

$$\frac{\partial u_1}{\partial t} + u_1 \frac{\partial u_1}{\partial x} + \left[1 - \frac{g'}{g}\theta^n\right] \theta^n \frac{\partial h}{\partial x} = 0, \tag{2.45}$$

$$\frac{\partial h}{\partial t} + \frac{\partial}{\partial x}(h u_1) = 0, \tag{2.46}$$

$$\frac{\mathrm{d}\theta}{\mathrm{d}t} = Q(t). \tag{2.47}$$

If we further refine this model to the case of weak stratification we get the *weakly stratified deep ambient layer* model as

$$\frac{\partial u_1}{\partial t} + u_1 \frac{\partial u_1}{\partial x} + \theta^n \frac{\partial h}{\partial x} = 0, \tag{2.48}$$

$$\frac{\partial h}{\partial t} + \frac{\partial}{\partial x}(h u_1) = 0, \tag{2.49}$$

$$\frac{\mathrm{d}\theta}{\mathrm{d}t} = Q(t). \tag{2.50}$$

This same model can be obtained from the weakly stratified model represented by equations (2.33)–(2.37) by letting $H \to \infty$ with $h = \mathrm{O}(1)$ in that system.

3. Preliminary analysis

The system given by Eqs. (2.21)–(2.24) and (2.27) is too complex to solve exactly. To make analytical progress we will focus on the *weakly stratified* and *weakly stratified deep ambient layer* systems. The advantage offered by these reduced, or simplified, systems is that they are better suited for analytical examination while at the same time retaining the essential physics of the full system. In this section analyses will be carried out on these two systems.

We begin by casting the systems (2.42)–(2.43) and (2.48)–(2.49) in conservation form. Setting $H = 1$ (thus $0 < h < 1$) and defining the vector

$$\mathbf{U} = \begin{bmatrix} u_1 \\ h \end{bmatrix}, \tag{3.1}$$

enables us to express the equations in the generic form

$$\frac{\partial \mathbf{U}}{\partial t} + \frac{\partial}{\partial x}\mathbf{F}(\mathbf{U}, t) = \mathbf{0}, \tag{3.2}$$

where the flux vector $\mathbf{F}$ is given by

$$\mathbf{F} = \begin{bmatrix} \frac{1}{2}u_1^2 + \eta(u_1, h, \theta) \\ u_1 h \end{bmatrix}, \tag{3.3}$$

for the weakly stratified model (using (2.40) for $\eta(u_1, h, \theta)$) and

$$\mathbf{F} = \begin{bmatrix} \frac{1}{2}u_1^2 + \theta^n h \\ u_1 h \end{bmatrix}, \tag{3.4}$$

for the weakly stratified deep ambient layer model.

The eigenvalues associated with the Jacobian matrix $\partial\mathbf{F}/\partial\mathbf{U}$ are:

$$\lambda^{\pm} = \frac{u_1(1-2h)}{1-h} \pm \frac{1}{1-h}\sqrt{h(1-h)[(1-h)^2\theta^n - u_1^2]}, \tag{3.5}$$

for the weakly stratified model and

$$\lambda^{\pm} = u_1 \pm \sqrt{\theta^n h}, \tag{3.6}$$

for the weakly stratified deep ambient layer model. These systems are classified as hyperbolic where $\lambda^{\pm}$ are real [17]. By inspecting the eigenvalues it is clear that the region of hyperbolicity corresponding to the weakly stratified model can be represented in the $u_1 - h$ plane by the set of all points (u_1, h) satisfying

$$(1-h)^2\theta^n - u_1^2 \geqslant 0. \tag{3.7}$$

The points (u_1, h) lying on and inside the triangular region bounded by the vertices located at $(u_1, h) = (-\sqrt{\theta^n(t)}, 0), (\sqrt{\theta^n(t)}, 0), (0, 1)$ satisfy the above condition. This triangular region will evolve in time due to the term $\theta^n(t)$. The weakly stratified deep ambient layer model, on the other hand, is always hyperbolic.

It has been shown that the weakly stratified system can be expressed compactly in characteristic form as

$$\frac{\mathrm{d}u_1}{\mathrm{d}t} + \left\{ \frac{u_1}{1-h} \pm \sqrt{\frac{1-h}{h}}\sqrt{\theta^n - \frac{u_1^2}{(1-h)^2}} \right\} \frac{\mathrm{d}h}{\mathrm{d}t} = 0$$

$$\text{along } \frac{\mathrm{d}x}{\mathrm{d}t} = \frac{u_1(1-2h)}{1-h} \pm \sqrt{h(1-h)}\sqrt{\theta^n - \frac{u_1^2}{(1-h)^2}}, \tag{3.8}$$

which can be further simplified to

$$\frac{\mathrm{d}}{\mathrm{d}t}\left\{\arcsin\left(\frac{u_1}{(1-h)\sqrt{\theta^n}}\right)\pm\arcsin\left(2\left(h-\frac{1}{2}\right)\right)\right\}=-\frac{nu_1Q(t)}{2\theta\sqrt{(1-h)^2\theta^n-u_1^2}}$$

$$\text{along}\ \frac{\mathrm{d}x}{\mathrm{d}t}=\frac{u_1(1-2h)}{1-h}\pm\sqrt{h(1-h)}\sqrt{\theta^n-\frac{u_1^2}{(1-h)^2}}. \tag{3.9}$$

Similarly, the weakly stratified deep ambient layer system can be reduced to

$$\frac{\mathrm{d}}{\mathrm{d}t}\left\{u_1\pm2\sqrt{\theta^nh}\right\}=\pm\frac{n\sqrt{\theta^nh}Q(t)}{\theta}\quad\text{along}\ \frac{\mathrm{d}x}{\mathrm{d}t}=u_1\pm\sqrt{\theta^nh}. \tag{3.10}$$

Lastly, in order to assess the nonlinear nature of the characteristic fields $\lambda^{\pm}(\mathbf{U})$ we must consider the quantity

$$\mathrm{grad}_{\mathbf{u}}\lambda^{\pm}\cdot\mathbf{r}^{\pm}, \tag{3.11}$$

where $\mathbf{r}^{\pm}$ are the corresponding right eigenvectors. The characteristic field is classified as *genuinely nonlinear* if the above quantity is nonzero and *linearly degenerate* if it is zero [17]. It is a straightforward exercise to show that the characteristic fields for the weakly stratified system are locally linearly degenerate about the state $u_1=0, h=\frac{1}{2}$. This will be further investigated numerically.

The weakly stratified deep ambient layer system (2.48)–(2.50) admits similarity solutions for the following choices of the heat flux $Q(t)$:

$$Q(t)=Q_0, \tag{3.12}$$

$$Q(t)=-k\theta. \tag{3.13}$$

The case given by (3.12) represents a constant heat flux which could be due to solar radiation for $Q_0>0$, while the case (3.13) corresponds to Newton's Law of Cooling where the surrounding temperature is fixed at T_0. With $Q(t)$ specified according to (3.12) or (3.13), Eq. (2.50) can be easily solved using the initial condition given by (2.28). The following solutions emerge for $\theta(t)$:

$$\theta(t)=Q_0\left(t+\frac{1}{Q_0}\right), \tag{3.14}$$

$$\theta(t)=\mathrm{e}^{-kt}, \tag{3.15}$$

for the cases (3.12), (3.13) respectively.

We next seek self-similar solutions having the form

$$u_1(x,t)=\tau^aV(\xi),\quad h(x,t)=\tau^bF(\xi),\quad \xi=x\tau^c,\quad \tau=t+\frac{1}{Q_0}, \tag{3.16}$$

for case (3.12) and

$$u_1(x,t)=\mathrm{e}^{at}V(\xi),\quad h(x,t)=\mathrm{e}^{bt}F(\xi),\quad \xi=x\mathrm{e}^{ct}, \tag{3.17}$$

for case (3.13). When these forms are substituted into (2.48)–(2.49) ordinary differential equations for V and F will result provided that

$$a+c=-1,\quad 2a-b=n, \tag{3.18}$$

for case (3.12) and

$$a + c = 0, \quad a - b - c = -nk, \tag{3.19}$$

for case (3.13). If we further impose the constraint that the volume of the surface gravity current remains constant (that is, we ignore the effect of thermal expansion to leading order) then

$$\int_0^\infty h(x,t)\,\mathrm{d}x = h_* x_0, \tag{3.20}$$

according to (2.32). This yields the additional requirement that

$$b = c, \tag{3.21}$$

for both cases (3.12) and (3.13). Combining (3.18)–(3.19) and (3.21) leads to

$$a = \frac{n-1}{3}, \quad b = c = -\frac{(n+2)}{3}, \tag{3.22}$$

for case (3.12) and

$$a = -\frac{nk}{3}, \quad b = c = \frac{nk}{3}, \tag{3.23}$$

for case (3.13).

The solution for V satisfying the impermeability condition (2.29) is

$$V(\xi) = \frac{(n+2)}{3}\,\xi, \tag{3.24}$$

for case (3.12) and

$$V(\xi) = -\frac{nk}{3}\,\xi, \tag{3.25}$$

for case (3.13). Similarly, the solution for F satisfying the jump condition

$$\frac{1}{2}\dot{x}_f^2 = \theta^n h(x_f, t), \tag{3.26}$$

where x_f denotes the location of the shock front and $\dot{x}_f$ the shock speed, is given by

$$F(\xi) = \frac{(n+2)}{18 Q_0^n}\,[(2n+1)\xi_f^2 - (n-1)\xi^2], \tag{3.27}$$

for case (3.12) and

$$F(\xi) = \frac{n^2 k^2}{18}\,[2\xi_f^2 - \xi^2], \tag{3.28}$$

for case (3.13). Here, ξ_f corresponds to the shock front x_f via equations (3.16)–(3.17). Further, ξ_f can be related to the initial volume by applying (3.20) and replacing the upper limit with x_f. The following expressions are obtained:

$$\xi_f = 3\left(\frac{2Q_0^n h_* x_0}{(n+2)(5n+4)}\right)^{1/3}, \tag{3.29}$$

for case (3.12) and

$$\xi_f = 3\left(\frac{2h_* x_0}{5n^2 k^2}\right)^{1/3}, \tag{3.30}$$

for case (3.13).

We point out that for the case (3.12) having $n = 0$ (i.e. constant density difference with $Q_0 = 1$), (3.24), (3.27) and (3.29) are in full agreement with those of Fannelop and Waldman [8] and Hoult [13]. Also, we add that for the case (3.12) with $n = 1$

$$\dot{x}_f = (2Q_0 h_* x_0)^{1/3}, \tag{3.31}$$

that is the shock propagates at constant speed, while for $n = 2$

$$\dot{x}_f = 4\left(\frac{Q_0^2 h_* x_0}{28}\right)^{1/3} \tau^{1/3}, \tag{3.32}$$

the shock speed increases with time. In contrast, for constant density difference the shock speed decreases with time. Examining the similarity solution for case (3.13) we observe that $\dot{x}_f \to 0$ as $t \to \infty$ for $n > 0$. This suggests that the gravity current eventually comes to rest. This is physically plausible since in the limit of large t the upper layer approaches the same density and temperature as the ambient fluid.

4. Numerical results and discussion

We next discuss the technique used to numerically integrate the equations. The numerical solution will be used to validate the weakly stratified and weakly stratified deep ambient layer models, as well as the analytical results. As in the previous section, we set $H = 1$ and so the parameter h_* now represents the initial depth ratio.

In obtaining numerical results to nonlinear hyperbolic conservation laws the difficulty lies mainly in accurately approximating discontinuous solutions. One of the major challenges is eliminating the spurious numerical oscillations associated with second-order accurate schemes. An effective strategy is to limit the antidiffusive term in the numerical flux in such a way as to obtain a TVD (total variation diminishing) scheme which yields solutions that are second-order accurate on smooth regions, and converge in a non-oscillatory manner to the correct entropy solutions. It turns out, however, that most TVD schemes, when applied to systems of conservation laws, require a specific linearization of the Jacobian of the flux vector, and a subsequent decomposition into characteristic fields. For large, highly coupled systems as the system given by (2.21)–(2.24), this approach is not practical. The alternative is to use a component-wise scheme which does not involve the Jacobian matrix. A widely used scheme is MacCormack's method, which is a second-order shock-capturing scheme. To deal with the numerical oscillations, an artificial viscosity term, such as the one proposed by Lapidus [16], can easily be imbedded into the scheme. Introducing artificial viscosity guarantees convergence to the correct entropy solution, as well as dampens the oscillations. However, the restriction imposed on it by the desired second-order accuracy prevents the complete elimination of oscillations.

To obtain oscillation-free solutions to our problem, we employed a second-order accurate TVD scheme arising from a modification to MacCormack's scheme recently advanced by Yu and Liu [27]. The modification is made by adding a flux limiter to the antidiffusive term. Depending on the structure of the solution, the limiter switches the scheme from MacCormack to that of Beam-Warming. It is known that the Beam-Warming scheme and that of MacCormack produce oscillations on opposite sides of a discontinuity (see Le Veque [18]). The elimination of oscillations then results from the solution dependent interchange between these two schemes. In the linear case, Yu and Liu's method

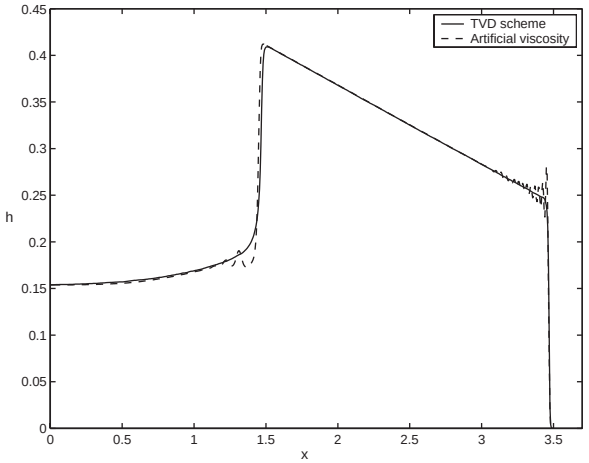

Fig. 2. The thickness of the gravity current obtained using the full model with $n = 1$, $Q_0 = 1$, $g'/g = 0.01$, $h_* = 0.9$, and $s = 0$, at $t = 3$.

reduces to the TVD scheme devised by Sweby [25] by adding a flux limiter to the Lax-Wendroff method. For our problem, the results are in excellent agreement with those obtained by the standard MacCormack's scheme using Lapidus' artificial viscosity. As illustrated by the plot presented in Fig. 2, the TVD scheme yields oscillation-free solutions while maintaining a shock resolution equivalent to that provided by the standard MacCormack scheme. Numerical experiments yield close agreement between the results obtained using space increments of $\Delta x = 0.005$ with those using $\Delta x = 0.01$. This serves as an indication of the convergence of the numerical technique as the grid spacing is refined. The numerical results presented in this paper were calculated using $\Delta x = 0.005$ except for those cases which involved a large space domain, where $\Delta x = 0.01$ was used instead. In all of our calculations the scheme proved to be stable provided the time step was selected to be between 10^{-3} and 10^{-4}.

Figs. 3a and b illustrate the evolution of the gravity current as it spreads over the ambient layer for the case $Q(t) = 1$ (i.e. $Q_0 = 1$ and $\theta(t) = t + 1$). The case presented in Fig. 3a corresponds to a relatively shallow ambient layer ($h_* = 0.9$), while in Fig. 3b the ambient layer is relatively deep ($h_* = 0.3$). The evolution revealed in Fig. 3a indicates the formation of an internal bore behind the head of the gravity current which is evident from $t = 3$ to $t = 7$. The bore is generated when the reverse flow in the ambient layer reaches the wall at $x = 0$ causing a sudden change in the flow rate of the gravity current. The bore propagates downstream along the interface between the two layers and eventually catches up to the front, which then results in the collapse of the head portion of the gravity current. If the ambient layer is deep, this reverse flow is insufficient to generate a rear bore. Instead, a long depression wave propagates along the interface towards the front.

The dependence of the general shape and evolution of the gravity current on the initial depth ratio is similar to that observed in previous studies [5,24] involving the spread of bottom gravity currents as a result of a constant density difference. An interesting difference, however, exists in the structure of the head region. As shown in Fig. 3a, the shape of the head region appears to be trapezoidal instead of rectangular as observed in [5,24]. We found that by considering a constant

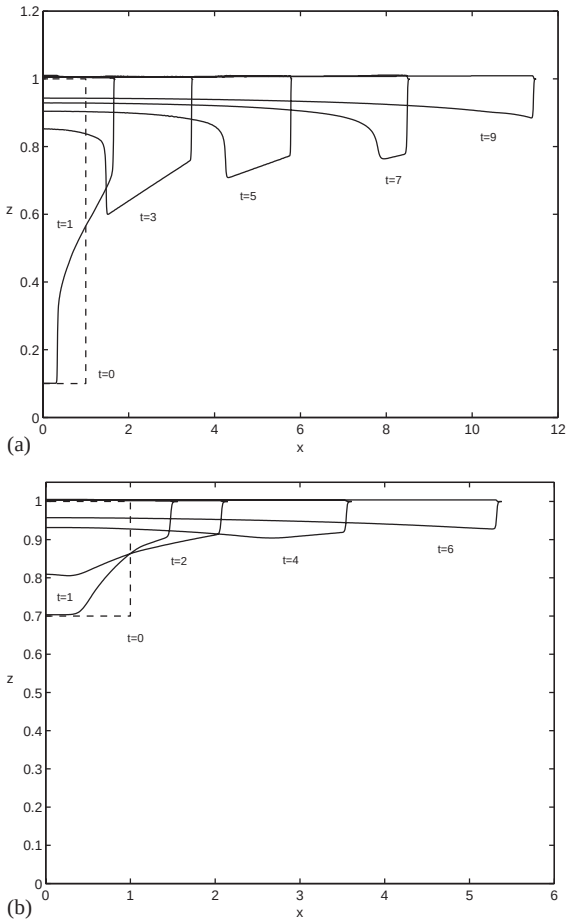

Fig. 3. (a) The evolution of the two-layer system obtained using the full model with $n = 1$, $Q_0 = 1$, $g'/g = 0.01$, $h_* = 0.9$, and $s = 0$. (b) The evolution of the two-layer system obtained using the full model with $n = 1$, $Q_0 = 1$, $g'/g = 0.01$, $h_* = 0.3$, and $s = 0$.

density difference in the current model (obtained by setting $Q(t) = 0$), this yielded profiles with rectangular head regions. This suggests that the trapezoidal structure of the head is an artifact of the time varying density difference. This trapezoidal head shape has been observed in other situations where the density difference varies in time. For example, in the works of Bonnecaze et al. [4] and Moodie et al. [22] where particle deposition from turbidity currents provided for a time-varying bulk density the current profile displayed a pronounced trapezoidal head shape. We also note on comparing Figs. 3a and b that the larger the value of h_* the faster the gravity current advances. Since the rate at which the temperature rises and hence the density changes is independent of the local current thickness in our model this difference in the rate of advance must be a result of the heightened reverse flow in the denser ambient fluid due to increased values of h_*. This same phenomenon has been observed for fixed density two layer bottom flows as well [5].

The effect of rising temperature and hence decreasing density on the flow rate of the upper current can readily be discerned from both Figs. 3a and b where the rate of advance is seen to increase

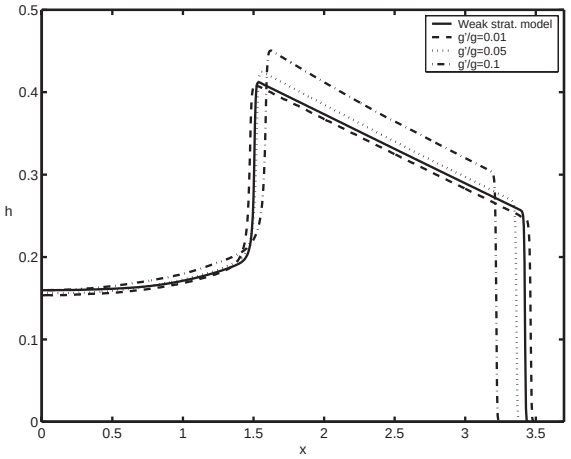

Fig. 4. The thickness of the gravity current obtained using the full model and the weakly stratified model with $n = 1$, $Q_0 = 1$, and $h_* = 0.9$ at $t = 3$.

with time and increased buoyancy force. For example, in Fig. 3a the difference between the rate of advance over the two time intervals between $t = 3$ and 5 and that for $t = 7$ and 9 shows an increase on the order of 26.3%. Similar increases with time are displayed in Fig. 3b although the overall rate of advance for this smaller release volume is not as great. Figs. 3a and b provide snapshots of the evolution of the two-layer system. Of special interest, though, is the gravity current itself, and in particular how the various parameters in the problem influence its development. The evolution of the gravity current can best be tracked by examining the variation of its thickness along its length. This is best portrayed by a graph of h as a function of x which will be presented in the remaining plots, with the exception of Fig. 11.

Comparisons between the numerical solutions of the full model equations (2.21)–(2.24) and (2.27) with those obtained from the weakly stratified and weakly stratified deep ambient layer models will now be drawn. As before, these comparisons were made using $Q(t) = 1$. The results shown in Fig. 4 verify that as $g'/g \to 0$ the solution to the full model approaches that of the weakly stratified model, as expected. Good agreement was also observed between the solutions of the full model and those of the weakly stratified deep ambient layer model, for small values of the parameter h_*. This is illustrated in Fig. 5. We point out that the results plotted in Figs. 4 and 5 were obtained using $n = 1$. Similar agreement was found when $n = 2$.

We next present comparisons between the similarity and the numerical solutions. A comparison with the similarity solution is given in Fig. 6 for the case $Q(t) = 1$. It is clearly seen that, as expected, the agreement improves as time increases. Shown in Fig. 7a is the evolution of the gravity current for the case of Newton's Law of Cooling using the weakly stratified deep ambient layer model with $n = 1$. The similarity solution is not included since it predicts a spike to form at the origin. Although the similarity solution gives poor agreement with the numerical solution, it does correctly predict two important features: the forming of a spike and the slowing down of the current, both of which are illustrated in Fig. 7a. Thus, the similarity solution fails only in its prediction of the front location. The formation of the spike is due to the variation in the horizontal velocity within the gravity

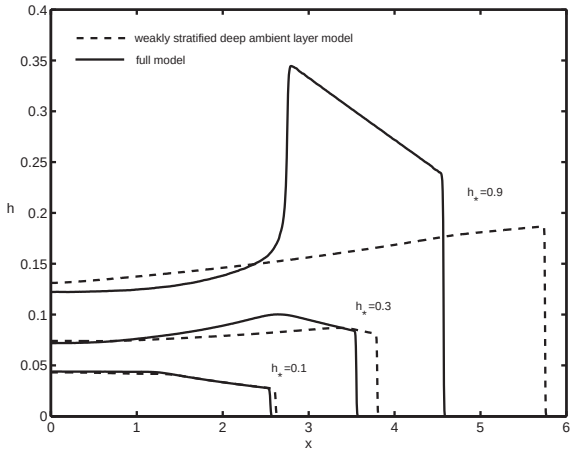

Fig. 5. The thickness of the gravity current with $n = 1$, $Q_0 = 1$, and $g'/g = 0.01$ (for the full model) at $t = 4$.

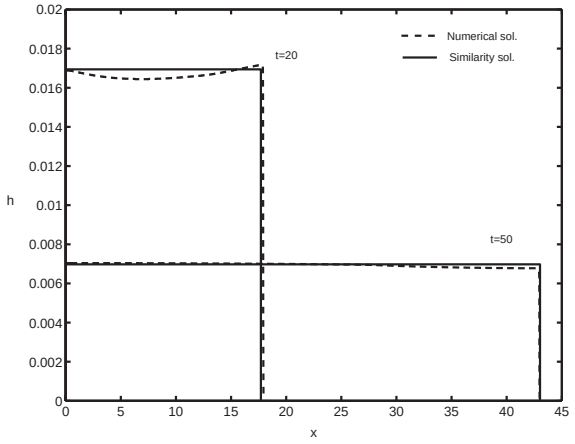

Fig. 6. Comparison of numerical and similarity solutions with $n = 1$, $Q_0 = 1$, and $h_* = 0.3$.

current. Illustrated in Fig. 7b is the horizontal velocity distribution along the length of the current at various times. It reveals that the maximum horizontal velocity is attained not at the front of the current, as in the heating case, but rather at an interior point. Because of the decrease in velocity as the front is approached, this causes fluid to accumulate near the front which consequently leads to the observed spike. Since the buoyancy force will diminish in time as a result of the cooling of the upper layer, the front will decelerate and this will further contribute to the piling up of fluid near the front of the gravity current. The ultimate form of the spike for very large times will resemble a delta function having an infinite height with vanishing thickness. Lastly, the characteristic 'peaking' of the gravity current at its leading edge displayed in Fig. 7a as it loses density contrast with its surroundings and slows has been observed in other situations involving the loss of buoyancy force with time. For example, in the case of particle-driven flows with sedimenting particles [23].

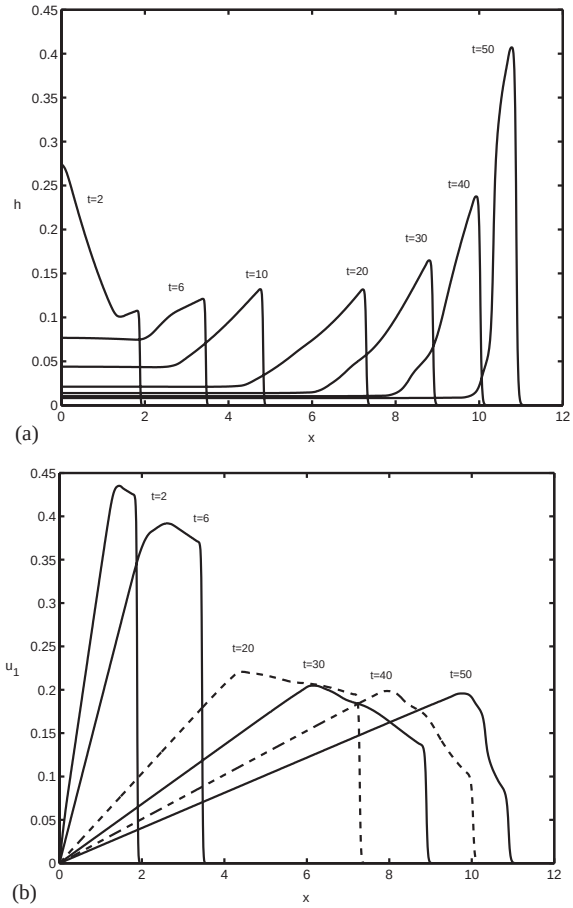

Fig. 7. (a) Evolution of the gravity current with $n = 1$, $k = 0.1$, and $h_* = 0.3$. (b) Evolution of the horizontal velocity distribution with $n = 1$, $k = 0.1$, and $h_* = 0.3$.

As a final comparison, Fig. 8 illustrates the influence of the initial depth ratio parameter h_* on the formation of the rear bore. The numerical results suggest that the rear bore forms when $h_* \gtrsim 0.5$. This is consistent with our earlier finding, namely that

$$\mathrm{grad}_{\mathbf{u}}\lambda^{\pm} \cdot \mathbf{r}^{\pm} = 0$$

when $h_* = \frac{1}{2}$ which denotes local linear degeneracy.

A comparison between the gravity currents having the power law indexes $n = 1$ and 2 is presented in Fig. 9 for the case $Q(t) = 1$. We see that the basic structure and development of the gravity current is similar for both $n = 1$ and 2. The only noticeable difference is in the rate of spreading, which is due to the difference in front speeds. This difference arises because of an increased rate of density decrease for the case $n = 2$ owing to the nonlinear dependence of the density on temperature differences. The effect of increasing the value of Q_0 can be assessed by comparing the evolutions in Figs. 9 and 10. It can be seen that Q_0 does not affect the evolutionary structure of the current, it

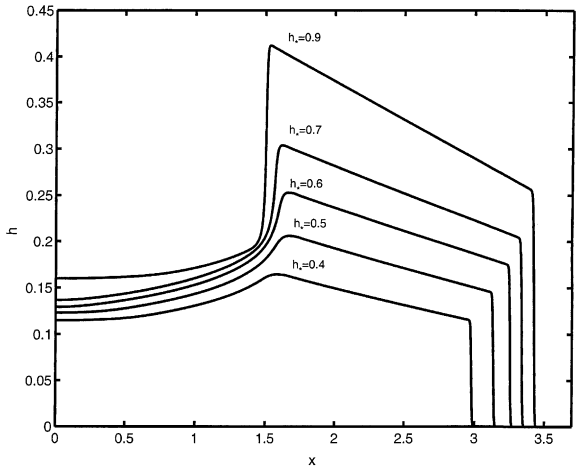

Fig. 8. The influence of h_* on the gravity current obtained using the weakly stratified model with $n = 1$ and $Q_0 = 1$ at $t = 3$.

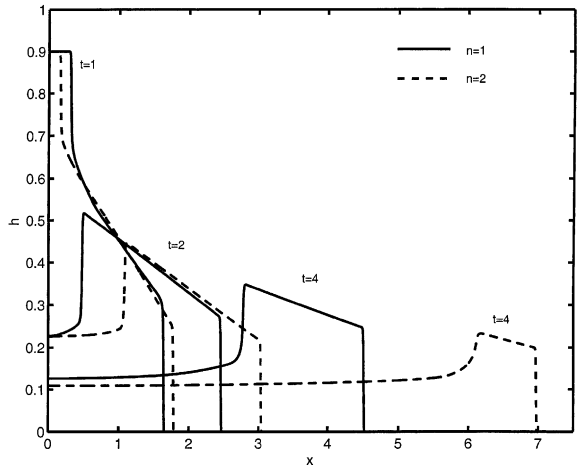

Fig. 9. Comparison of the evolution of the gravity current with $n = 1$ and 2 obtained using the weakly stratified model with $Q_0 = 1$ and $h_* = 0.9$.

also appears to only affect the rate at which spreading occurs. In Fig. 11 we show the evolution of the gravity current relative to the ambient layer with a sloping bottom having

$$f(x) = 1 - e^{-x}.$$

Contrasting this evolution with that in Fig. 3a for a flat bottom, we observe that there is an important difference in the progression of the rear bore. In the case with a sloping bottom a rear bore is generated, however it appears to gradually dissipate, unlike in the flat bottom case where the bore persists until it reaches the front of the current. The results displayed in Fig. 11 would suggest that as the current moves out into deeper surroundings the role of release flow in maintaining the

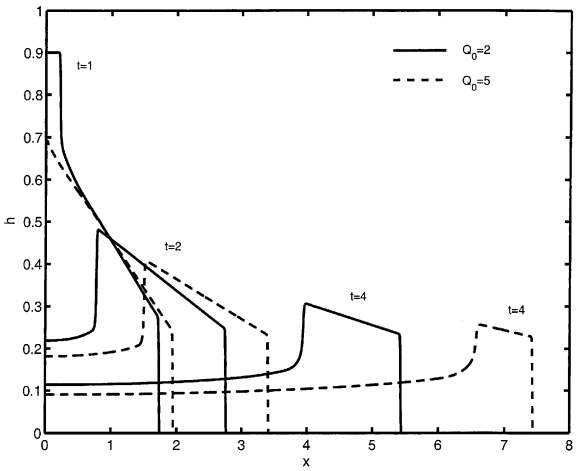

Fig. 10. The evolution of the thickness of the gravity current obtained using the weakly stratified model with $n = 1$ and $h_* = 0.9$.

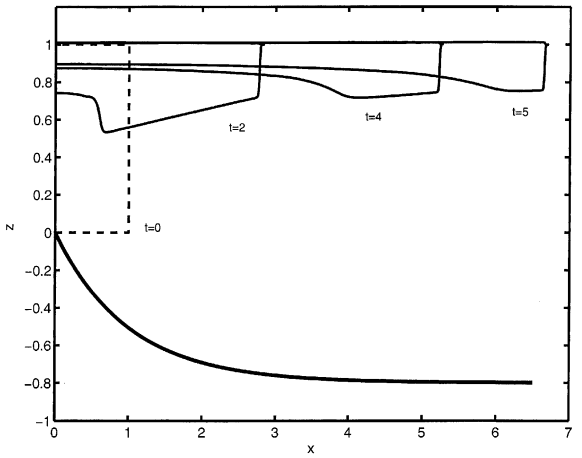

Fig. 11. The evolution of the two-layer system obtained using the full model with $n = 1$, $Q_0 = 1$, $g'/g = 0.01$, $h_* = 1$, and $s = 0.8$.

rear bore is diminished. The plots in Fig. 12 indicate that this effect is accentuated as the bottom becomes steeper (i.e. as s is increased). Judging from the positions of the fronts, these results also suggest that the rate of spreading of the gravity current increases with s, which appears to happen at the expense of having a thinner head. We point out that for all the cases in Fig. 12 the same initial volume was released. The initial position of the fluid in all cases is indicated by the dash line shown in Fig. 11.

As a final comment regarding the case $n = 2$, we point out that this serves as a simple model for the thermal bar phenomenon observed in dimictic lakes. The thermal bar arises from the fact that the shallow, near-shore regions of a lake tend to warm and cool faster than the deeper, off-shore regions,

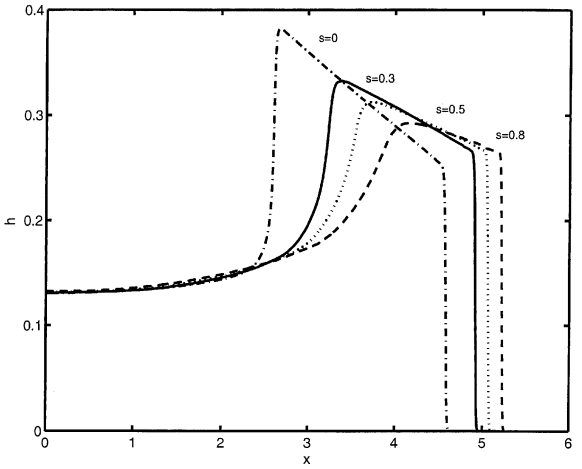

Fig. 12. Comparison of the evolution of the thickness of the gravity current with bottom slope obtained using the full model with $n = 1$, $Q_0 = 1$, $g'/g = 0.01$, and $h_* = 1$ at $t = 4$.

as well as due to the existence of a density maximum in the equation of state. For water near the temperature of maximum density of 4°C, the equation of state is well approximated by Eq. (2.1) with $n = 2$ [6]. The 4°C isotherm is termed the thermal bar; it advances out from the shore and will eventually reach the deepest parts of the lake, after which the lake becomes stratified. Consequently, a double cell circulation pattern with downwelling occurring in the vicinity of the 4°C isotherm is produced. The thermal bar appears in the spring as a lake is being heated above 4°C and re-appears in the fall when a lake cools below 4°C. Many investigations have been devoted to the thermal bar, some of which include [9,28] and [3,7,10–12,14]. Since $g'/g = 0$ corresponds to the start-up of the thermal bar from zero initial stratification, the weakly stratified model presented here could provide insightful information into the initial development of the thermal bar.

5. Weakly nonlinear analysis

In this section we will further investigate the formation of the rear bore behind the head of the gravity current as observed in the numerical simulations for $h_* \gtrsim 0.5$. Since shock formation is a nonlinear phenomenon, we employ a weakly nonlinear analysis, similar to that in [5], on the weakly stratified model equations given by (2.42) and (2.43) with $H = 1$. We first expand the flow variables about the basic state given by $(u, h) = (0, h_*)$, taking $u \equiv u_1$, which corresponds to the release configuration. The weakly stratified model equations can then be reduced to the following quadratically nonlinear system:

$$\frac{\partial \hat{u}}{\partial t} + \frac{(1 - 3h_*)}{(1 - h_*)}\,\hat{u}\,\frac{\partial \hat{u}}{\partial x} + \theta^n (1 - h_* - \hat{h})\,\frac{\partial \hat{h}}{\partial x} = 0, \tag{5.1}$$

$$\frac{\partial \hat{h}}{\partial t} + (h_* + \hat{h})\,\frac{\partial \hat{u}}{\partial x} + \hat{u}\,\frac{\partial \hat{h}}{\partial x} = 0, \tag{5.2}$$

where the hat denotes the deviation from the basic state $(0, h_*)$. Eqs. (5.1) and (5.2) can be combined to yield a single equation given by (dropping the hats)

$$h_{tt} - h_*(1-h_*)\theta^n h_{xx} = -(uh)_{xt} - h_*\theta^n(hh_x)_x + \frac{(1-3h_*)h_*}{(1-h_*)}(uu_x)_x, \tag{5.3}$$

with subscripts denoting partial differentiation.

In the analysis that follows we will illustrate the procedure for the specific case $Q(t) = Q_0$ and $n = 2$ where $0 < Q_0 = \varepsilon \ll 1$, so that

$$\theta(t) = 1 + \varepsilon t. \tag{5.4}$$

This particular choice corresponds to a case discussed in some detail in this study and also minimizes the algebra involved. Other values of n can be tackled in a similar manner. The reason for the restriction $Q_0 \ll 1$ is twofold. As alluded to earlier, the hydraulic model imposes constraints on the rate of heating/cooling. This restriction guarantees that Eq. (5.3) will remain valid for sufficiently large times. Secondly, the heating/cooling rate brings in another time scale which then suggests introducing the slow time variable $T = \varepsilon t$. As a final note we add that the condition $Q_0 \ll 1$ is consistent with the spirit of this study, in that we are looking at the enhancement of gravity driven flows brought on by heating/cooling superimposed on an existing stratified system.

The next step involves the defining of better-suited coordinates given by

$$\xi = x - c(t)t, \quad \eta = x + c(t)t, \quad T = \varepsilon t, \tag{5.5}$$

where the phase speed, $c(t)$, is given by

$$c(t) = c_0\left(1 + \frac{\varepsilon}{2}t\right), \quad c_0 = \sqrt{h_*(1-h_*)}. \tag{5.6}$$

In addition, we expand the variables in the following series

$$h = \varepsilon h^{(0)}(\xi, \eta, T) + \varepsilon^2 h^{(1)}(\xi, \eta, T) + \cdots, \tag{5.7}$$

$$u = \varepsilon u^{(0)}(\xi, \eta, T) + \varepsilon^2 u^{(1)}(\xi, \eta, T) + \cdots\ . \tag{5.8}$$

To transform equation (5.3) we make use of

$$\begin{aligned} \partial_x &= \partial_\eta + \partial_\xi, \\ \partial_t &= c_0(1+T)(\partial_\eta - \partial_\xi) + \varepsilon\partial_T, \\ \partial_{xt}^2 &= c_0(1+T)(\partial_{\eta\eta}^2 - \partial_{\xi\xi}^2) + \varepsilon\partial_T(\partial_\eta + \partial_\xi), \end{aligned} \tag{5.9}$$

then to leading order we obtain:

$$h_{\eta\xi}^{(0)} = 0, \tag{5.10}$$

$$c_0(\partial_\eta - \partial_\xi)u^{(0)} = -(1-h_*)(1+T)(\partial_\eta + \partial_\xi)h^{(0)}, \tag{5.11}$$

where (5.11) follows from (5.1). These can be easily solved to give

$$h^{(0)} = \phi(\xi, T) + \psi(\eta, T), \tag{5.12}$$

$$u^{(0)} = \frac{(1-h_*)(1+T)}{c_0}(\phi(\xi, T) - \psi(\eta, T)). \tag{5.13}$$

Employing these results we are able to find the correction $h^{(1)}$. After some algebra we obtain

$$-4c_0^2 h^{(1)}_{\eta\xi} = A(\xi, T) + B(\xi, \eta, T) + C(\eta, T), \tag{5.14}$$

where

$$A(\xi, T) = \frac{2c_0}{(1+T)}\,\phi_{T\xi} + \frac{3}{2}(1-2h_*)(\phi^2)_{\xi\xi}, \tag{5.15}$$

$$B(\xi, \eta, T) = -(1-2h_*)[\phi\psi_{\eta\eta} + \psi\phi_{\xi\xi} + 2\psi_\eta\phi_\xi], \tag{5.16}$$

$$C(\eta, T) = -\frac{2c_0}{(1+T)}\,\psi_{T\eta} + \frac{3}{2}(1-2h_*)(\psi^2)_{\eta\eta}. \tag{5.17}$$

To ensure that $h^{(1)}$ remains bounded as $\xi, \eta \to \pm\infty$ we impose $A = 0$ and $C = 0$ as solvability conditions. Since the equations $A = 0$ and $C = 0$ are very similar, we will present only the details for the solution of $A = 0$.

Integrating $A = 0$ with respect to ξ gives

$$\phi_T + \frac{3(1-2h_*)(1+T)}{2c_0}\,\phi\phi_\xi = 0, \tag{5.18}$$

where ϕ is assumed to have compact support. If we let $\phi(\xi, 0) = f(\xi)$ represent the initial condition, then the solution to (5.18) can be expressed implicitly in parametric form in terms of the parameter s as

$$\phi(\xi, T) = f(s) \quad \text{along } \xi = \frac{3(1-2h_*)}{4c_0}[(1+T)^2 - 1]f(s) + s. \tag{5.19}$$

Shock formation occurs when $|\phi_\xi| \to \infty$ where

$$\phi_\xi = \frac{4c_0 f'(s)}{4c_0 + 3(1-2h_*)f'(s)[(1+T)^2 - 1]}, \tag{5.20}$$

which becomes infinite when

$$T(s) = -1 \pm \sqrt{1 - K(s)}, \quad K(s) = \frac{4c_0}{3(1-2h_*)f'(s)}. \tag{5.21}$$

Thus, a shock will form for $T > 0$ when $K(s) < 0$. For $f'(s) > 0$ (i.e. the back side of the rightward propagating smooth initial wave) this will happen provided $h_* > \frac{1}{2}$ and confirms our numerical observations. The first breaking time, T_B, will be given by

$$T_B = \min_s [T(s)]. \tag{5.22}$$

A similar conclusion would be drawn by considering the equation $C = 0$.

We conclude this section with a brief discussion of the case of constant cooling (i.e. $Q(t) = Q_0$ where $-1 \ll Q_0 = \varepsilon < 0$). This analysis still predicts that a rear bore should form for $h_* > \frac{1}{2}$ and has also been confirmed numerically. The only point worth mentioning about this case is that the analysis is restricted to the interval $0 < T < 1$. This, however, makes physical sense since for $T > 1$ the upper layer becomes denser than the ambient layer and thus the configuration is unstable.

6. Concluding remarks

Discussed in this paper is the problem of a surface gravity current acted upon by a heat flux. The mathematical formulation was based on shallow-water theory for a two-layer fluid model. Under conditions of weak stratification and deep ambient layer thickness, three limiting models have been identified. These include the weakly stratified, deep ambient layer, and weakly stratified deep ambient layer models. These limiting models constitute a simplified system consisting of two equations for the upper layer velocity and thickness together with algebraic expressions for the remaining unknowns. Two types of results were obtained: analytical results using the simplified systems and numerical results using both the full and the simplified systems. The analyses carried out include similarity solutions to predict the long-term behaviour and a weakly nonlinear analysis to explain the rear bore formation. The numerical solutions, obtained by a recently-advanced numerical scheme for solving systems of nonlinear hyperbolic conservation laws, confirmed the analytical predictions and the validity of the simplified systems. A distinguished feature of these flows is the formation of a rear bore behind the head of the current for certain h_* ratios, similar in appearance to what has been observed with bottom boundary currents. Also, the head of the gravity current takes on a trapezoidal shape rather than the familiar rectangular shape reported in previous studies involving fixed density flows.

Acknowledgements

Financial support for this research was provided by the Natural Sciences and Engineering Research Council of Canada.

References

[1] N. Antar, T.B. Moodie, Weakly nonhydrostatic effects in compositionally-driven gravity flows, Stud. Appl. Math. 111 (2003) 239–267.
[2] T.B. Benjamin, Gravity currents and related phenomena, J. Fluid Mech. 31 (1968) 209–248.
[3] J.R. Bennett, Thermally driven lake currents during the spring and fall transition periods, Proceedings of the 14th Conference on Great Lakes Research, Ann Arbor, Michigan, 1971, pp. 535–544.
[4] R.T. Bonnecaze, H.E. Huppert, J.R. Lister, Particle-driven gravity currents, J. Fluid Mech. 250 (1993) 339–369.
[5] S.J.D. D'Alessio, T.B. Moodie, J.P. Pascal, G.E. Swaters, Gravity currents produced by sudden release of a fixed volume of heavy fluid, Stud. Appl. Math. 96 (1996) 359–385.
[6] H. Eklund, Freshwater: temperature of maximum density calculated from compressibility, Science 142 (1963) 1457–1458.
[7] G.H. Elliott, A mathematical study of the thermal bar, In: Proceedings of the 14th Conference on Great Lakes Research, Ann Arbor, Michigan, 1971, pp. 545–554.
[8] T.K. Fannelop, G.D. Waldman, Dynamics of oil slicks, AIAA J. 10 (1972) 506–510.
[9] D.E. Farrow, An asymptotic model for the hydrodynamics of the thermal bar, J. Fluid Mech. 289 (1995) 129–140.
[10] D.E. Farrow, A numerical model of the hydrodymanics of the thermal bar, J. Fluid Mech. 303 (1995) 279–295.
[11] D.E. Farrow, A model of the thermal bar in the rotating frame including vertically non-uniform heating, Environ. Fluid Mech. 2 (2002) 197–218.
[12] P.R. Holland, A. Kay, V. Botte, A numerical study of the dynamics of the riverine thermal bar in a deep lake, Environ. Fluid Mech. 1 (2001) 311–332.

[13] D.P. Hoult, Oil spreading on the sea, Ann. Rev. Fluid Mech. 4 (1972) 341–368.
[14] D.W. Hubbard, J.D. Spain, The structure of the early spring thermal bar in Lake Superior, Proceedings of the 16th Conference on Great Lakes Research, Ann Arbor, Michigan, 1973, pp. 735–742.
[15] P.K. Kundu, Fluid Mechanics, Academic Press, London, 1990.
[16] A. Lapidus, A detached shock calculation by second-order finite differences, J. Comput. Phys. 2 (1967) 154–177.
[17] P.D. Lax, Hyperbolic Systems of Conservation Laws and the Mathematical Theory of Shock Waves, SIAM, Philadelphia, PA, 1973.
[18] R. Le Veque, Numerical Methods for Conservation Laws, Birkhäuser, Basel, 1992.
[19] P.F. Linden, The fluid mechanics of natural ventilation, Ann. Rev. Fluid Mech. 31 (1999) 201–238.
[20] J. Malm, S. Zilitinkevich, Temperature distribution and current system in a convectively mixed lake, Bound. Layer Meteor. 71 (1994) 219–234.
[21] T.B. Moodie, J.P. Pascal, Non-hydraulic effects in particle-driven gravity currents in deep surroundings, Stud. Appl. Math. 107 (2001) 217–251.
[22] T.B. Moodie, J.P. Pascal, J.C. Bowman, Modeling sediment deposition patterns arising from suddenly released fixed-volume turbulent suspensions, Stud. Appl. Math. 105 (2000) 333–359.
[23] T.B. Moodie, J.P. Pascal, G.E. Swaters, Sediment transport and deposition from a two-layer fluid model of gravity currents on sloping bottoms, Stud. Appl. Math. 100 (1998) 215–244.
[24] J.W. Rottman, J.E. Simpson, Gravity currents produced by instantaneous releases of a heavy fluid in a rectangular channel, J. Fluid Mech. 135 (1983) 95–110.
[25] P.K. Sweby, High resolution schemes using flux limiters for hyperbolic conservation laws, SIAM J. Numer. Anal. 21 (1984) 995–1011.
[26] T. von Kármán, The engineer grapples with nonlinear problems, Bull. Amer. Math. Soc. 46 (1940) 615–683.
[27] H. Yu, Y. Liu, A second-order accurate, component-wise TVD scheme for nonlinear, hyperbolic conservation laws, J. Comput. Phys. 173 (2001) 1–16.
[28] S.S. Zilitinkevich, K.D. Kreiman, A.Y. Terzhevik, The thermal bar, J. Fluid Mech. 236 (1992) 27–42.